JOPSS
JAEA Originated Papers Searching System

日本原子力研究開発機構機関リポジトリ
Japan Atomic Energy Agency Institutional Repository

Title	Inclusive and exclusive measurements of B decays to χ_{c1} and χ_{c2} at Belle
Author(s)	Bhardwaj V., Tanida Kiyoshi, Belle Collaboration, 197 of others
Citation	Physical Review D,93(5),p.052016_1-052016_13
Text Version	Publisher's Version
URL	https://jopss.jaea.go.jp/search/servlet/search?5057544
DOI	https://doi.org/10.1103/PhysRevD.93.052016
Right	© 2016 American Physical Society

Japan Atomic Energy Agency

Inclusive and exclusive measurements of B decays to χ_{c1} and χ_{c2} at Belle

V. Bhardwaj,[61,*] K. Miyabayashi,[45] E. Panzenböck,[10,45] K. Trabelsi,[15,11] A. Frey,[10] A. Abdesselam,[64] I. Adachi,[15,11] H. Aihara,[71] S. Al Said,[64,29] K. Arinstein,[3,51] D. M. Asner,[53] H. Atmacan,[40] V. Aulchenko,[3,51] T. Aushev,[42] R. Ayad,[64] V. Babu,[65] I. Badhrees,[64,28] S. Bahinipati,[17] A. M. Bakich,[63] A. Bala,[54] V. Bansal,[53] E. Barberio,[39] B. Bhuyan,[18] J. Biswal,[24] A. Bobrov,[3,51] A. Bondar,[3,51] A. Bozek,[49] M. Bračko,[37,24] T. E. Browder,[14] D. Červenkov,[4] V. Chekelian,[38] A. Chen,[46] B. G. Cheon,[13] K. Chilikin,[41] R. Chistov,[41] K. Cho,[30] V. Chobanova,[38] S.-K. Choi,[12] Y. Choi,[62] D. Cinabro,[77] J. Dalseno,[38,66] M. Danilov,[41] Z. Doležal,[4] D. Dutta,[65] S. Eidelman,[3,51] H. Farhat,[77] J. E. Fast,[53] T. Ferber,[7] O. Frost,[7] B. G. Fulsom,[53] V. Gaur,[65] N. Gabyshev,[3,51] S. Ganguly,[77] A. Garmash,[3,51] R. Gillard,[77] R. Glattauer,[21] Y. M. Goh,[13] P. Goldenzweig,[26] B. Golob,[34,24] D. Greenwald,[67] J. Haba,[15,11] P. Hamer,[10] K. Hayasaka,[44] H. Hayashii,[45] X. H. He,[55] W.-S. Hou,[48] T. Iijima,[44,43] K. Inami,[43] A. Ishikawa,[69] R. Itoh,[15,11] Y. Iwasaki,[15] I. Jaegle,[14] D. Joffe,[27] K. K. Joo,[5] T. Julius,[39] E. Kato,[69] P. Katrenko,[42] T. Kawasaki,[50] C. Kiesling,[38] D. Y. Kim,[60] J. B. Kim,[31] K. T. Kim,[31] M. J. Kim,[32] S. H. Kim,[13] Y. J. Kim,[30] K. Kinoshita,[6] B. R. Ko,[31] N. Kobayashi,[72] P. Kodyš,[4] S. Korpar,[37,24] P. Križan,[34,24] P. Krokovny,[3,51] T. Kuhr,[35] R. Kumar,[57] T. Kumita,[73] A. Kuzmin,[3,51] Y.-J. Kwon,[79] I. S. Lee,[13] C. Li,[39] Y. Li,[76] L. Li Gioi,[38] J. Libby,[19] D. Liventsev,[76,15] A. Loos,[61] P. Lukin,[3,51] M. Masuda,[70] D. Matvienko,[3,51] H. Miyata,[50] R. Mizuk,[41,42] G. B. Mohanty,[65] S. Mohanty,[65,75] A. Moll,[38,66] H. K. Moon,[31] R. Mussa,[23] E. Nakano,[52] M. Nakao,[15,11] T. Nanut,[24] Z. Natkaniec,[49] M. Nayak,[19] N. K. Nisar,[65] S. Nishida,[15,11] S. Ogawa,[68] S. Okuno,[25] G. Pakhlova,[42] B. Pal,[6] C. W. Park,[62] H. Park,[32] T. K. Pedlar,[36] R. Pestotnik,[24] M. Petrič,[24] L. E. Piilonen,[76] C. Pulvermacher,[26] M. V. Purohit,[61] J. Rauch,[67] E. Ribežl,[24] M. Ritter,[38] A. Rostomyan,[7] H. Sahoo,[14] Y. Sakai,[15,11] S. Sandilya,[65] L. Santelj,[15] T. Sanuki,[69] Y. Sato,[43] V. Savinov,[56] O. Schneider,[33] G. Schnell,[1,16] C. Schwanda,[21] Y. Seino,[50] D. Semmler,[8] K. Senyo,[78] O. Seon,[43] M. E. Sevior,[39] V. Shebalin,[3,51] C. P. Shen,[2] T.-A. Shibata,[72] J.-G. Shiu,[48] B. Shwartz,[3,51] F. Simon,[38,66] J. B. Singh,[54] Y.-S. Sohn,[79] A. Sokolov,[22] E. Solovieva,[42] M. Starič,[24] J. Stypula,[49] M. Sumihama,[9] T. Sumiyoshi,[73] U. Tamponi,[23,74] K. Tanida,[59] Y. Teramoto,[52] M. Uchida,[72] S. Uehara,[15,11] T. Uglov,[42] Y. Unno,[13] S. Uno,[15,11] P. Urquijo,[39] Y. Usov,[3,51] C. Van Hulse,[1] P. Vanhoefer,[38] G. Varner,[14] A. Vinokurova,[3,51] V. Vorobyev,[3,51] C. H. Wang,[47] M.-Z. Wang,[48] P. Wang,[20] X. L. Wang,[76] M. Watanabe,[50] Y. Watanabe,[25] S. Wehle,[7] E. Won,[31] J. Yamaoka,[53] S. Yashchenko,[7] H. Ye,[7] Y. Yook,[79] C. Z. Yuan,[20] Y. Yusa,[50] Z. P. Zhang,[58] V. Zhilich,[3,51] V. Zhulanov,[3,51] and A. Zupanc[24]

(Belle Collaboration)

[1]*University of the Basque Country UPV/EHU, 48080 Bilbao*
[2]*Beihang University, Beijing 100191*
[3]*Budker Institute of Nuclear Physics SB RAS, Novosibirsk 630090*
[4]*Faculty of Mathematics and Physics, Charles University, 121 16 Prague*
[5]*Chonnam National University, Kwangju 660-701*
[6]*University of Cincinnati, Cincinnati, Ohio 45221*
[7]*Deutsches Elektronen–Synchrotron, 22607 Hamburg*
[8]*Justus-Liebig-Universität Gießen, 35392 Gießen*
[9]*Gifu University, Gifu 501-1193*
[10]*II. Physikalisches Institut, Georg-August-Universität Göttingen, 37073 Göttingen*
[11]*SOKENDAI (The Graduate University for Advanced Studies), Hayama 240-0193*
[12]*Gyeongsang National University, Chinju 660-701*
[13]*Hanyang University, Seoul 133-791*
[14]*University of Hawaii, Honolulu, Hawaii 96822*
[15]*High Energy Accelerator Research Organization (KEK), Tsukuba 305-0801*
[16]*IKERBASQUE, Basque Foundation for Science, 48013 Bilbao*
[17]*Indian Institute of Technology Bhubaneswar, Satya Nagar 751007*
[18]*Indian Institute of Technology Guwahati, Assam 781039*
[19]*Indian Institute of Technology Madras, Chennai 600036*
[20]*Institute of High Energy Physics, Chinese Academy of Sciences, Beijing 100049*
[21]*Institute of High Energy Physics, Vienna 1050*
[22]*Institute for High Energy Physics, Protvino 142281*
[23]*INFN, Sezione di Torino, 10125 Torino*
[24]*J. Stefan Institute, 1000 Ljubljana*
[25]*Kanagawa University, Yokohama 221-8686*
[26]*Institut für Experimentelle Kernphysik, Karlsruher Institut für Technologie, 76131 Karlsruhe*
[27]*Kennesaw State University, Kennesaw, Georgia 30144*

 © 2016 American Physical Society

[28]*King Abdulaziz City for Science and Technology, Riyadh 11442*
[29]*Department of Physics, Faculty of Science, King Abdulaziz University, Jeddah 21589*
[30]*Korea Institute of Science and Technology Information, Daejeon 305-806*
[31]*Korea University, Seoul 136-713*
[32]*Kyungpook National University, Daegu 702-701*
[33]*École Polytechnique Fédérale de Lausanne (EPFL), Lausanne 1015*
[34]*Faculty of Mathematics and Physics, University of Ljubljana, 1000 Ljubljana*
[35]*Ludwig Maximilians University, 80539 Munich*
[36]*Luther College, Decorah, Iowa 52101*
[37]*University of Maribor, 2000 Maribor*
[38]*Max-Planck-Institut für Physik, 80805 München*
[39]*School of Physics, University of Melbourne, Victoria 3010*
[40]*Middle East Technical University, 06531 Ankara*
[41]*Moscow Physical Engineering Institute, Moscow 115409*
[42]*Moscow Institute of Physics and Technology, Moscow Region 141700*
[43]*Graduate School of Science, Nagoya University, Nagoya 464-8602*
[44]*Kobayashi-Maskawa Institute, Nagoya University, Nagoya 464-8602*
[45]*Nara Women's University, Nara 630-8506*
[46]*National Central University, Chung-li 32054*
[47]*National United University, Miao Li 36003*
[48]*Department of Physics, National Taiwan University, Taipei 10617*
[49]*H. Niewodniczanski Institute of Nuclear Physics, Krakow 31-342*
[50]*Niigata University, Niigata 950-2181*
[51]*Novosibirsk State University, Novosibirsk 630090*
[52]*Osaka City University, Osaka 558-8585*
[53]*Pacific Northwest National Laboratory, Richland, Washington 99352*
[54]*Panjab University, Chandigarh 160014*
[55]*Peking University, Beijing 100871*
[56]*University of Pittsburgh, Pittsburgh, Pennsylvania 15260*
[57]*Punjab Agricultural University, Ludhiana 141004*
[58]*University of Science and Technology of China, Hefei 230026*
[59]*Seoul National University, Seoul 151-742*
[60]*Soongsil University, Seoul 156-743*
[61]*University of South Carolina, Columbia, South Carolina 29208*
[62]*Sungkyunkwan University, Suwon 440-746*
[63]*School of Physics, University of Sydney, New South Wales 2006*
[64]*Department of Physics, Faculty of Science, University of Tabuk, Tabuk 71451*
[65]*Tata Institute of Fundamental Research, Mumbai 400005*
[66]*Excellence Cluster Universe, Technische Universität München, 85748 Garching*
[67]*Department of Physics, Technische Universität München, 85748 Garching*
[68]*Toho University, Funabashi 274-8510*
[69]*Tohoku University, Sendai 980-8578*
[70]*Earthquake Research Institute, University of Tokyo, Tokyo 113-0032*
[71]*Department of Physics, University of Tokyo, Tokyo 113-0033*
[72]*Tokyo Institute of Technology, Tokyo 152-8550*
[73]*Tokyo Metropolitan University, Tokyo 192-0397*
[74]*University of Torino, 10124 Torino*
[75]*Utkal University, Bhubaneswar 751004*
[76]*CNP, Virginia Polytechnic Institute and State University, Blacksburg, Virginia 24061*
[77]*Wayne State University, Detroit, Michigan 48202*
[78]*Yamagata University, Yamagata 990-8560*
[79]*Yonsei University, Seoul 120-749*

(Received 8 December 2015; published 29 March 2016)

We report inclusive and exclusive measurements for χ_{c1} and χ_{c2} production in B decays. We measure $\mathcal{B}(B \to \chi_{c1} X) = (3.03 \pm 0.05(\text{stat}) \pm 0.24(\text{syst})) \times 10^{-3}$ and $\mathcal{B}(B \to \chi_{c2} X) = (0.70 \pm 0.06(\text{stat}) \pm 0.10(\text{syst})) \times 10^{-3}$. For the first time, χ_{c2} production in exclusive B decays in the modes $B^0 \to \chi_{c2}\pi^- K^+$ and $B^+ \to \chi_{c2}\pi^+\pi^- K^+$ has been observed, along with first evidence for the $B^+ \to \chi_{c2}\pi^+ K^0_S$

[*]Present address: Indian Institute of Science Education and Research Mohali, SAS Nagar 140306.

decay mode. For χ_{c1} production, we report the first observation in the $B^+ \to \chi_{c1}\pi^+\pi^-K^+$, $B^0 \to \chi_{c1}\pi^+\pi^-K^0_S$ and $B^0 \to \chi_{c1}\pi^0\pi^-K^+$ decay modes. Using these decay modes, we observe a difference in the production mechanism of χ_{c2} in comparison to χ_{c1} in B decays. In addition, we report searches for $X(3872)$ and $\chi_{c1}(2P)$ in the $B^+ \to (\chi_{c1}\pi^+\pi^-)K^+$ decay mode. The reported results use 772×10^6 $B\bar{B}$ events collected at the $\Upsilon(4S)$ resonance with the Belle detector at the KEKB asymmetric-energy e^+e^- collider.

DOI: 10.1103/PhysRevD.93.052016

I. INTRODUCTION

Belle reported the first observation of χ_{c2} production in B meson decays with an inclusive measurement [1]. The $\chi_{cJ}(J = 1, 2)$ [2] momentum distributions in the $\Upsilon(4S)$ rest frame indicate that most of the χ_{c2} mesons come from nontwo-body B decays [1,3]. Still, there have been only a few searches for exclusive B decays with a χ_{c2} in the final state, $B^+ \to \chi_{c2}K^+$ [4] and $B^0 \to \chi_{c2}K^*(892)^0$ [5–7]. The $B^+ \to \chi_{c2}K^{(*)}$ decays are found to be highly suppressed with respect to the similar χ_{c1} processes [8]. The suppression can be explained in the framework of the factorization in two-body B decays [9], where χ_{c2} production is allowed only when one takes into account final-state interactions. Due to angular momentum conservation, $J^{PC} = 0^{-+}$, 1^{--} and 1^{++} are favored while 0^{++}, 2^{++}, 2^{--} and so on are suppressed.

A study of the multibody B decay modes with χ_{c1} and χ_{c2} in the final state is important to understand the detailed dynamics of B meson decays. Further, one can search for charmonium/charmoniumlike exotic states in one of the intermediate final states such as $\chi_{cJ}\pi$ and $\chi_{cJ}\pi\pi$. For example, looking at the $\chi_{c1}\pi^+\pi^-$ invariant mass spectrum in $B \to \chi_{c1}\pi^+\pi^-K$ decays, one can search for $\chi_{c1}(2P)$ and/or $X(3872)$. The quantum numbers of the narrow exotic resonance $X(3872)$ have been determined to be $J^{PC} = 1^{++}$ [10–12]. One plausible interpretation is an admixture of a $D^0\bar{D}^{*0}$ molecule and a conventional charmonium with the same J^{PC}, the yet-unseen $\chi_{c1}(2P)$ [13]. The $\chi_{c1}(2P)$ component may have a substantial decay rate to $\chi_{c1}\pi^+\pi^-$ because of no obvious conflict in quantum numbers and observations of dipion transitions between χ_{bJ} states in the bottomonium system. In the case in which $X(3872)$ is not a mixed state and hence $\chi_{c1}(2P)$ is a physically observable state, its decay to $\chi_{c1}\pi^+\pi^-$ would still be expected. Its mass is predicted to be about 3920 MeV/c^2, assuming that it lies between $\chi_{c2}(2P)$ and the $X(3915)$ that is interpreted as $\chi_{c0}(2P)$ by PDG [8].

Using the $\chi_{cJ} \to J/\psi\gamma$ modes, we report on the inclusive branching fractions ($\mathcal{B}$) of $B \to \chi_{cJ}X$ decays and the exclusive reconstruction of multibody B decays to χ_{cJ} in order to search for still-undiscovered intermediate states.

II. DATA SAMPLE AND DETECTOR

We use a data sample of 772×10^6 $B\bar{B}$ events collected with the Belle detector [14] at the KEKB asymmetric-energy e^+e^- collider operating at the $\Upsilon(4S)$ resonance [15]. The Belle detector is a large-solid-angle spectrometer, which includes a silicon vertex detector (SVD), a 50-layer central drift chamber (CDC), an array of aerogel threshold Cherenkov counters (ACC), time-of-flight scintillation counters (TOF), and an electromagnetic calorimeter (ECL) comprised of 8736 CsI(Tl) crystals located inside a superconducting solenoid coil that provides a 1.5 T magnetic field. An iron flux return located outside the coil is instrumented to detect K^0_L mesons and identify muons. The detector is described in detail elsewhere [14]. Two inner detector configurations were used. A first sample of 152×10^6 $B\bar{B}$ events was collected with a 2.0 cm radius beam pipe and a three-layer SVD, while the remaining 620×10^6 $B\bar{B}$ pairs were collected with a 1.5 cm radius beam pipe, a four-layer silicon detector and modified CDC (the cathode part of the CDC replaced by a compact small cell-type drift chamber) [16].

III. EVENT SELECTION

We reconstruct inclusive χ_{cJ} from B decays. To suppress continuum background, we exploit the $\Upsilon(4S)$ decay topology. For the events passing the Belle standard hadronic event selection [17], we require the ratio of the second to zeroth Fox-Wolfram moment [18] to be less than 0.5. Charged tracks are required to originate from the vicinity of the interaction point (IP): the distance of closest approach to the IP is required to be within 3.5 cm along the beam direction and within 1.0 cm in the transverse plane. Photons are reconstructed from the energy deposition in the ECL by requiring no matching with any extrapolated charged track. To further avoid photons coming from neutral hadrons, we reject the photon candidate if the ratio of the energy deposited in the central array of 3×3 ECL cells to that deposited in the enclosing array of 5×5 cells is less than 0.85.

We use EVTGEN [19] with QED final-state radiation by PHOTOS [20] for the generation of Monte Carlo (MC) simulation events. A GEANT-based [21] MC simulation is used to model the response of the detector and determine the efficiency of the signal reconstruction.

The J/ψ meson is reconstructed via its decays to $\ell^+\ell^-$ ($\ell = e$ or μ) and selected by the invariant mass $M_{\ell\ell}$. For the dimuon mode, $M_{\ell\ell}$ is given by the

invariant mass $M_{\mu^+\mu^-}$; for the dielectron mode, the four-momenta of all photons within 50 mrad with respect to the original direction of the e^+ or e^- tracks are included in $M_{\ell\ell} \equiv M_{e^+e^-(\gamma)}$ to reduce the radiative tail. The reconstructed invariant mass of the J/ψ candidates is required to satisfy $2.95\ \mathrm{GeV}/c^2 < M_{e^+e^-(\gamma)} < 3.13\ \mathrm{GeV}/c^2$ or $3.03\ \mathrm{GeV}/c^2 < M_{\mu^+\mu^-} < 3.13\ \mathrm{GeV}/c^2$. For the selected J/ψ candidates, a vertex-constrained fit is applied to the charged tracks and then a mass-constrained fit is performed to improve its momentum resolution. The χ_{c1} and χ_{c2} candidates are reconstructed by combining a J/ψ candidate with a photon having an energy larger than 100 MeV.

IV. INCLUSIVE B DECAYS TO χ_{cJ}

A. Branching fraction measurement

To reduce combinatorial background coming from $\pi^0 \to \gamma\gamma$, we use a likelihood function that distinguishes an isolated photon from π^0 decays using the photon-pair invariant mass, the photon laboratory-frame energy, and the laboratory-frame polar angle with respect to the beam direction [22]. We reject both photons of a pair whose π^0 likelihood probability is larger than 0.3. Applying this cut, combinatorial background is reduced by 56.9% (59.1%) with a signal loss of 26.5% (39.9%) for χ_{c2} (χ_{c1}).

To identify the signal, we use the distribution of the $J/\psi\gamma$ invariant mass $M_{J/\psi\gamma}$ and extract the signal yield from a binned maximum likelihood fit. The signal of χ_{cJ} is described by a double-sided Crystal Ball function [23,24], which accommodates the tails of the mass distribution. The function's left (right) side tail parameters n_l (n_r) and α_l (α_r) are fixed to the values obtained from MC-simulated events. For $B \to \chi_{c1}X$, all other shape parameters are floated in the fit whereas, for $B \to \chi_{c2}X$, they are fixed using the mass difference $(m_{\chi_{c2}} - m_{\chi_{c1}})$ from Ref. [8] and the resolution ratio between χ_{c1} and χ_{c2}, $\sigma_{\chi_{c2}}/\sigma_{\chi_{c1}}$, determined from MC simulations. The combinatorial background component is modeled with a third-order Chebyshev polynomial.

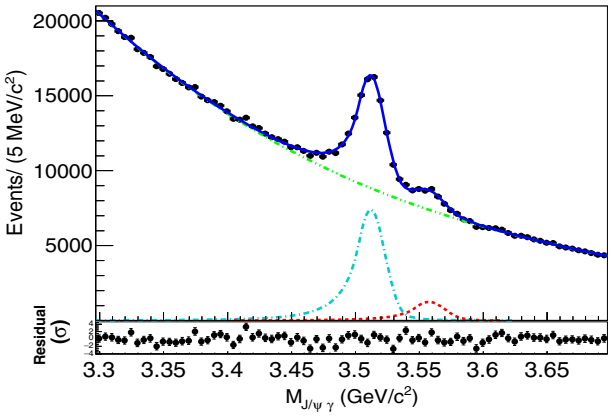

FIG. 1. $M_{J/\psi\gamma}$ distribution of the $B \to \chi_{cJ}(\to J/\psi(\to \ell^+\ell^-)\gamma)X$ decays in data. The curves show the signal (cyan dash dotted for χ_{c1} and red dashed for χ_{c2}) and the background component (green dash double dotted for combinatorial) as well as the overall fit (blue solid). The lower plot shows the pull of the residuals with respect to the fit.

Figure 1 shows the fit of the $M_{J/\psi\gamma}$ distribution for $\chi_{c1}X$ and $\chi_{c2}X$ decays in the range of $[3.297, 3.697]\ \mathrm{GeV}/c^2$. The fit returns a reduced χ^2 of 1.3 with a p value of 0.0123 and a yield of 51353 ± 614 events for the χ_{c1} and 9651 ± 446 events for the χ_{c2}, where the errors are statistical.

The reconstruction efficiencies for the inclusive $B \to \chi_{c1}X$ and $B \to \chi_{c2}X$ decays are estimated to be 24.2% and 25.9%, respectively. The efficiency is estimated using simulated multibody B decays, $B \to \chi_{cJ}K(n\pi)$, where the number of pions n varies from 0 to 4 over the entire $p^*_{\chi_{cJ}}$ range; it is averaged with proper weighting according to the distribution of $p^*_{\chi_{cJ}}$ in data.

We use the 2014 world-average values [8] for secondary daughter branching fractions $\mathcal{B}(J/\psi \to l^+l^-) = (11.932 \pm 0.004)\%$, $\mathcal{B}(\chi_{c1} \to J/\psi\gamma) = (33.9 \pm 1.2)\%$, and $\mathcal{B}(\chi_{c2} \to J/\psi\gamma) = (19.2 \pm 0.7)\%$.

We use the 89 fb^{-1} off-resonance data sample taken at 60 MeV below the $\Upsilon(4S)$ resonance to estimate the contribution of χ_{cJ} particles that do not arise from B meson decays. From the fit to the $M_{J/\psi\gamma}$ distribution for that sample, we obtain 139 ± 38 (92 ± 38) signal events for χ_{c1} (χ_{c2}), corresponding to 1098 ± 300 (727 ± 300) signal events for $\chi_{c1}X$ ($\chi_{c2}X$) after proper scaling to the integrated luminosity at the $\Upsilon(4S)$ resonance. The scaled χ_{c1} and χ_{c2} continuum yields are subtracted from the on-resonance yields.

One also expects a contribution from "feed down" $B \to \chi_{cJ}X$ decays where the χ_{cJ} is from the cascade $B \to \psi'X \to \chi_{cJ}\gamma X$. To determine the rate for direct decays to the χ_{cJ} states, we subtract this feed down contribution, which is estimated using $\mathcal{B}(B \to \psi'X)$ and $\mathcal{B}(\psi' \to \chi_{cJ}\gamma)$ from Ref. [8].

The sources and estimates of the systematic uncertainties are summarized in Table I. A correction for small differences in the signal detection efficiency between MC

TABLE I. Summary of systematic uncertainties in the $B \to \chi_{cJ}X$ branching fraction.

	Uncertainty (%)	
Source	$B \to \chi_{c1}X$	$B \to \chi_{c2}X$
Lepton identification	2.3	2.3
PDF uncertainty	3.1	7.9
Secondary $\mathcal{B}$	3.6	3.7
Tracking efficiency	0.7	0.7
$N_{B\bar{B}}$	1.4	1.4
Photon efficiency	2.0	2.0
π^0 veto	1.2	1.2
$B \to \chi_{cJ}X$ modeling	4.0	4.0
ψ' feed down	1.0	3.0
Total	7.3	10.7

and data has been applied for the lepton identification requirements. Uncertainties in these corrections are included in the systematic error. The $e^+e^- \to e^+e^-\ell^+\ell^-$ and $J/\psi \to \ell^+\ell^-$ ($\ell = e$ or μ) samples are used to estimate the lepton identification correction. The uncertainty of the probability density function (PDF) shapes are obtained by varying all fixed parameters by $\pm 1\sigma$, fitting with different binning, and using a fourth-order polynomial for the background, then adding the changes in the yield in quadrature to get the systematic uncertainty. We perform a fit to the data by including the χ_{c0} component and find its statistical significance to be 1.7σ. We further add the signal yield difference for χ_{c1} or χ_{c2} with respect to the original fit to the PDF systematic uncertainty. Based on this, we get an uncertainty of 3.1% (7.9%) for $B \to \chi_{c1}X$ ($B \to \chi_{c2}X$). The uncertainties due to the secondary branching fractions are also taken into account. The uncertainty on the track finding efficiency is found to be 0.35% per track by comparing the data and MC for $D^* \to D^0\pi$ decay, where $D^0 \to \pi^+\pi^- K^0_S$ and $K^0_S \to \pi^+\pi^-$; here one of the π is allowed not to be reconstructed explicitly. For $N_{B\bar{B}}$, systematic uncertainty is estimated to be 1.4%. The uncertainty on the photon identification is estimated to be 2.0% from a sample of radiative Bhabha events. The systematic uncertainty associated with the difference of the π^0 veto between data and MC is estimated to be 1.2% from a study of the $B^\pm \to \chi_{c1}(\to J/\psi\gamma)K^\pm$ sample. The potential bias to extract signal yields of the χ_{cJ} is estimated by the MC from variation of the efficiency for the different decay modes bin by bin in the $p^*_{\chi_{cJ}}$ distribution. The efficiency change due to the unknown χ_{cJ} polarization is estimated using the $B^0 \to \chi_{c1}K^{*0}$ signal MC samples by varying the polarization over the allowed range. The sum of these two effects is 4.0%.

We measure the feed down-contaminated branching fractions $\mathcal{B}(B \to \chi_{c1}X)$ and $\mathcal{B}(B \to \chi_{c2}X)$ to be $(3.33 \pm 0.05 \pm 0.24) \times 10^{-3}$ and $(0.98 \pm 0.06 \pm 0.10) \times 10^{-3}$, respectively, where the first (second) error is statistical (systematic). After subtracting the feed down contribution, we obtain the pure inclusive branching fractions $\mathcal{B}(B \to \chi_{c1}X) = (3.03 \pm 0.05 \pm 0.24) \times 10^{-3}$ and $\mathcal{B}(B \to \chi_{c2}X) = (0.70 \pm 0.06 \pm 0.10) \times 10^{-3}$. In both cases, the systematic uncertainty dominates. We estimate the inclusive branching fractions according to the formula

$$\mathcal{B}(B \to \chi_{cJ}X) = \frac{N_{\rm sig} - N_{\rm off}}{\epsilon \times N_B \times \mathcal{B}(\chi_{cJ} \to J/\psi\gamma) \times \mathcal{B}(J/\psi \to \ell^+\ell^-) - \mathcal{B}(B \to \psi' X) \times \mathcal{B}(\psi' \to \chi_{cJ}\gamma)}.$$

Here, $N_{\rm sig}$ is the obtained signal yield, $N_{\rm off}$ is the estimated off-resonance contribution, ϵ is the reconstruction efficiency, N_B is the number of B mesons in the data sample and $\mathcal{B}$ is the branching fraction for the particular mode taken from [8].

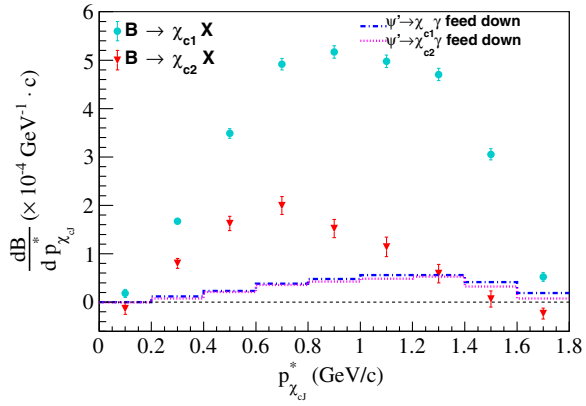

FIG. 2. Differential branching fractions $D\mathcal{B}(B \to \chi_{c1}X)$ with cyan circles (•) and $D\mathcal{B}(B \to \chi_{c2}X)$ with red triangles (▼) in each bin of $p^*_{\chi_{cJ}}$ extracted from the maximum likelihood fits performed with the ΔM distribution of the data sample for $B \to \chi_{cJ}(\to J/\psi\gamma)X$ after continuum suppression but without feed down subtraction. The ψ' feed down component (estimated from the MC simulation using ψ' momentum distribution presented in Ref. [3]) is shown by the blue dash-dotted (magenta dotted) line for χ_{c1} (χ_{c2}). The uncertainties in these plots are statistical only.

The ratio $\mathcal{R}_\mathcal{B} \equiv \mathcal{B}(B \to \chi_{c2}X)/\mathcal{B}(B \to \chi_{c1}X)$ is $(23.1 \pm 2.0 \pm 2.1)\%$. Here, most of the systematics cancel except for the PDF uncertainty (4.5%), secondary $\mathcal{B}$ (4.7%), unknown polarization (5.6%), and feed down (2.1%).

B. $p^*_{\chi_{cJ}}$ distribution

The distribution of the χ_{cJ} momentum in the e^+e^- center-of-mass (CM) frame, $p^*_{\chi_{cJ}}$, provides valuable insight into the production mechanism of the χ_{cJ}. To obtain the $p^*_{\chi_{cJ}}$ distribution, we fit the $M_{J/\psi\gamma}$ distribution in bins of $p^*_{\chi_{cJ}}$. We fix all of the signal parameters to the values obtained from the fit to the total and the resolution in each bin to the value obtained from the signal MC after MC/data correction. The background shape and normalization are floated in all fits. The fitted χ_{c1} and χ_{c2} yields are converted into differential branching fractions ($D\mathcal{B}$) after subtraction of the continuum contribution in each bin, estimated from the continuum data. In the absence of reliable bin by bin estimation of the feed down contribution, we do not apply feed down subtraction here. Efficiency corrections are applied to each bin. Figure 2 shows the resulting distributions of $D\mathcal{B}$ in bins of $p^*_{\chi_{cJ}}$. Suppression of the two-body decay of χ_{c2} is visible in the $p^*_{\chi_{cJ}}$ distribution. Most of the χ_{c2} production comes from three- or higher-body decays.

V. EXCLUSIVE RECONSTRUCTION

To further understand χ_{c1} and χ_{c2} production in B decays, we reconstruct the following exclusive B decays: $B^0 \to \chi_{cJ}\pi^- K^+$, $B^+ \to \chi_{cJ}\pi^+ K^0_S$, $B^+ \to \chi_{cJ}\pi^0 K^+$, $B^+ \to \chi_{cJ}\pi^+\pi^- K^+$, $B^0 \to \chi_{cJ}\pi^+\pi^- K^0_S$ and $B^0 \to \chi_{cJ}\pi^-\pi^0 K^+$ [25].

The χ_{c1} and χ_{c2} candidates are reconstructed as in the inclusive study except for a looser criterion to reduce the $\pi^0 \to \gamma\gamma$ background, requiring the π^0 likelihood probability to be less than 0.8. Applying this cut, the combinatorial background is reduced by 30%–35% with a signal loss of 6%–11% depending upon the mode of interest. The reconstructed invariant mass of the χ_{c1} (χ_{c2}) is required to satisfy $3.467\,\mathrm{GeV}/c^2 < M_{J/\psi\gamma} < 3.535\,\mathrm{GeV}/c^2$ ($3.535\,\mathrm{GeV}/c^2 < M_{J/\psi\gamma} < 3.579\,\mathrm{GeV}/c^2$). The selected mass windows correspond to $[-4.5\sigma, +2.8\sigma]$ for χ_{c1} and $[-1.5\sigma, +3.0\sigma]$ for χ_{c2} around their nominal mass. A mass-constrained fit is applied to the selected χ_{c1} and χ_{c2} candidates.

The combined information from the CDC, TOF and ACC is used to identify charged kaons and pions based on the K/π likelihood ratio, $R_K = \mathcal{L}_K/(\mathcal{L}_K + \mathcal{L}_\pi)$, where $\mathcal{L}_K$ and $\mathcal{L}_\pi$ are likelihood values for the kaon and pion hypotheses, respectively. A track is identified as a kaon if R_K is greater than 0.6; otherwise, it is classified as a pion. The kaon (pion) identification efficiency lies in the range of 87%–94% (94%–97%) while the probability of misidentifying a pion (kaon) as a kaon (pion) is 6.8%–10.4% (6.5%–7.0%), depending on the momentum range of kaons and pions. To ensure that tracks with low transverse momentum (p_T) with respect to the beam axis are included only once as they can curl up and result in duplicate tracks, criteria similar to those of Refs. [26,27] are used: duplicated tracks for charged pions with $p_T < 0.25$ GeV/c often appear as the track pair having $\cos\theta_{\mathrm{open}} > 0.95$ ($\cos\theta_{\mathrm{open}} < -0.95$) for same (opposite) charged tracks, where θ_{open} is the angle between the two tracks. Among those, when the difference between the absolute value of the momentum of the two tracks is less than 0.1 GeV/c, it is treated as a duplicate pair. Of the two such tracks, the one having the closest approach to the IP is retained.

K^0_S mesons are reconstructed by combining two oppositely charged pions with an invariant mass $M_{\pi^+\pi^-}$ lying between 482 and 514 MeV/c^2 ($\pm 6\sigma$ around the nominal mass of the K^0_S). The selected candidates are required to satisfy the quality criteria described in Ref. [28]. Pairs of photons are combined to form π^0 candidates within the mass range 120 MeV/c^2 $< M_{\gamma\gamma} <$ 150 MeV/c^2 ($\pm 3\sigma$ around the nominal mass of π^0). To reduce combinatorial background, the $\pi^0 \to \gamma\gamma$ candidates are also required to have an energy balance parameter $|E_1 - E_2|/(E_1 + E_2)$ smaller than 0.8, where E_1 (E_2) is the energy of the first (second) photon in the laboratory frame. For each selected π^0 candidate, a mass-constrained fit is performed to improve its momentum resolution.

To identify the B meson, two kinematic variables are used: the beam-constrained mass M_{bc} and the energy difference ΔE. The former is defined as $\sqrt{E^2_{\mathrm{beam}}/c^2 - (\sum_i \vec{p}_i)^2}/c$ and the latter as $\sum_i E_i - E_{\mathrm{beam}}$, where E_{beam} is the beam energy in the CM frame and p_i (E_i) is the momentum (energy) of the ith daughter particle in the CM frame; the summation is over all final-state particles used for reconstruction. We reject candidates having M_{bc} less than 5.27 GeV/c^2 or $|\Delta E| > 120$ MeV. In case of multiple B candidates, we use a statistic χ^2, defined as

$$\chi^2 = \chi^2_V + \chi^2_N + \left(\frac{M_{\chi_{cJ}} - m_{\chi_{cJ}}}{\sigma_{\chi_{cJ}}}\right)^2 + \left(\frac{M_{\mathrm{bc}} - m_B}{\sigma_{M_{\mathrm{bc}}}}\right)^2,$$

where χ^2_V is the reduced χ^2 returned by the vertex fit of all charged tracks, χ^2_N is the reduced χ^2 for the K^0_S or π^0 mass-constrained fit, $M_{\chi_{cJ}}$ is the reconstructed mass of χ_{cJ}, and $m_{\chi_{cJ}}$ and m_B are the nominal masses of the χ_{cJ} and B mesons, respectively. The resolution $\sigma_{M_{\mathrm{bc}}}$ of M_{bc}, estimated from the fit to data, is 3 MeV/c^2. The resolution $\sigma_{\chi_{c1}}$ ($\sigma_{\chi_{c2}}$) of χ_{c1} (χ_{c2}), is taken to be 9.5 MeV (10.5 MeV) from the inclusive measurements. The B candidate with the lowest χ^2 value is retained. The procedure to select the most probable B candidate is called best candidate selection (BCS). After the reconstruction, a mean of 1.1–2.7 B candidates per event is found, depending on the decay mode, and the BCS chooses the true candidate 75%–98% of the time.

We extract the signal yield from an unbinned extended maximum likelihood (UML) fit to the ΔE variable. The signal PDF is modeled by the sum of two Gaussians unless otherwise explicitly mentioned. The parameters of the wider Gaussian are fixed from MC simulations while the mean and the width of the core Gaussian are treated according to the B decay mode. For the $B \to \chi_{c1}X$ decay modes, the parameters of the core Gaussian are floated unless otherwise stated. For $B \to \chi_{c2}X$, the core Gaussian is fixed after a data/MC correction estimated from the $B \to \chi_{c1}X$ decay mode; otherwise, a correction from the other decay mode is implemented.

To study the background from events with a J/ψ, we use a large MC-simulated $B \to J/\psi X$ sample corresponding to 100 times the integrated luminosity of the data sample. The non-J/ψ (non χ_{cJ}) background is studied using $M_{\ell\ell}$ ($M_{J/\psi\gamma}$) sidebands in data. For $B \to \chi_{c1}X$, no significant peaking background is found. However, in the $B \to \chi_{c2}X$ modes, there can be a contamination from $B \to \chi_{c1}X$ because of its larger branching fraction. We call this effect $B \to \chi_{c1}X$ cross feed. Since we apply a mass-constrained fit for $\chi_{c2} \to J/\psi\gamma$ candidates, this cross feed tends to cluster around $\Delta E = +50$ MeV. This peaking background is parametrized by a Gaussian whose yield and parameters are fixed from the signal MC study after applying a MC/data correction estimated from the $B \to \chi_{c1}X$ decay mode. The flat background in all decay modes is modeled with a Chebyshev first-order polynomial unless otherwise explicitly mentioned. For the $B \to \chi_{c1}X$ decay modes, the PDF comprises the signal PDF and a flat background; for

$B \to \chi_{c2}X$ decay modes, the PDF comprises the signal PDF, the $B \to \chi_{c1}X$ cross feed and a flat background.

To understand the intermediate states, we examine the background-subtracted $M_{\chi_{cJ}\pi}$, $M_{K\pi}$, $M_{\chi_{cJ}\pi\pi}$, $M_{K\pi\pi}$, and $M_{\pi\pi}$ distributions for the decay mode of interest. We perform a UML fit to the ΔE distribution and use the ${}_s\mathcal{P}lot$ formalism [29] to project signal events in the distribution.

The efficiency (ϵ) for each decay mode is estimated using MC simulation generated over the whole phase space. In the absence of information regarding the intermediate state and a proper model for each decay mode, we divide the sample according to the $M_{Kn\pi}$ and $M_{\chi_{cJ}n\pi}$ distributions, where $n \in \{1, 2\}$ is the number of pions, so that each bin indexed by i has equal statistics. The efficiency estimated in each bin (ϵ_i) using MC simulation is then weighted by the signal yield of the bin to provide the final efficiency $\epsilon = \sum_i w_i \epsilon_i$, where $w_i =$ yield in ith bin / total yield. In decay modes having no significant signal, the efficiency is simply estimated using MC simulation generated over the whole phase space as distribution is unknown. We calibrate this efficiency by the difference between MC simulation and data, as described later. The so-estimated efficiency for the decay mode of interest lies between 4.3% and 18.0%, depending upon the final states used for the reconstruction.

A. $B \to \chi_{cJ}\pi K$

To study χ_{cJ} production in three-body B decays, we use charged and neutral kaons and pions to reconstruct the B decay mode of interest: $B^0 \to \chi_{cJ}\pi^- K^+$, $B^+ \to \chi_{cJ}\pi^+ K^0_S$ and $B^+ \to \chi_{cJ}\pi^0 K^+$. The signal is identified using kinematic requirements on ΔE and $M_{\rm bc}$. Among the events containing B candidates, 10%, 16% and 22% have multiple candidates in the $B^0 \to \chi_{cJ}\pi^- K^+$, $B^+ \to \chi_{cJ}\pi^+ K^0_S$ and $B^+ \to \chi_{cJ}\pi^0 K^+$ modes, respectively. The aforementioned BCS procedure is used to select the B candidate in such events.

The UML fit to the ΔE distribution for the $B^0 \to \chi_{cJ}\pi^- K^+$ and $B^+ \to \chi_{cJ}\pi^+ K^0_S$ decay modes is shown in Figs. 3(a)–3(d). For $B^+ \to \chi_{cJ}\pi^0 K^+$ decays, the signal is modeled by the sum of a Gaussian and a logarithmic Gaussian [30]. For $B^+ \to \chi_{c1}\pi^0 K^+$ decays, the mean and width of the core Gaussian are floated and the remaining parameters are fixed according to MC; for $B^+ \to \chi_{c2}\pi^0 K^+$ decays, all parameters are fixed after applying the data/MC correction estimated from the $B^+ \to \chi_{c1}\pi^0 K^+$ decay mode. No peaking background is expected in the $B^+ \to \chi_{c1}\pi^0 K^+$ decay mode while, in $B^+ \to \chi_{c2}\pi^0 K^+$, feed down from $B^+ \to \chi_{c1}\pi^0 K^+$ is expected and is modeled by a Gaussian PDF (whose yield and all parameters are fixed from MC-simulation study). The rest of the background is combinatorial and modeled using a first-order Chebyshev polynomial. The fit to the ΔE distribution for $B^+ \to \chi_{cJ}\pi^0 K^+$ is shown in Figs. 3(e)–3(f).

We obtain 2774 ± 66 (206 ± 25), 770 ± 35 (76 ± 15) and 803 ± 70 (17.5 ± 28.4) signal events for the $B^0 \to \chi_{c1}\pi^- K^+$ ($B^0 \to \chi_{c2}\pi^- K^+$), $B^+ \to \chi_{c1}\pi^+ K^0_S$ ($B^+ \to \chi_{c2}\pi^+ K^0_S$) and $B^+ \to \chi_{c1}\pi^0 K^+$ ($B^+ \to \chi_{c2}\pi^0 K^+$)

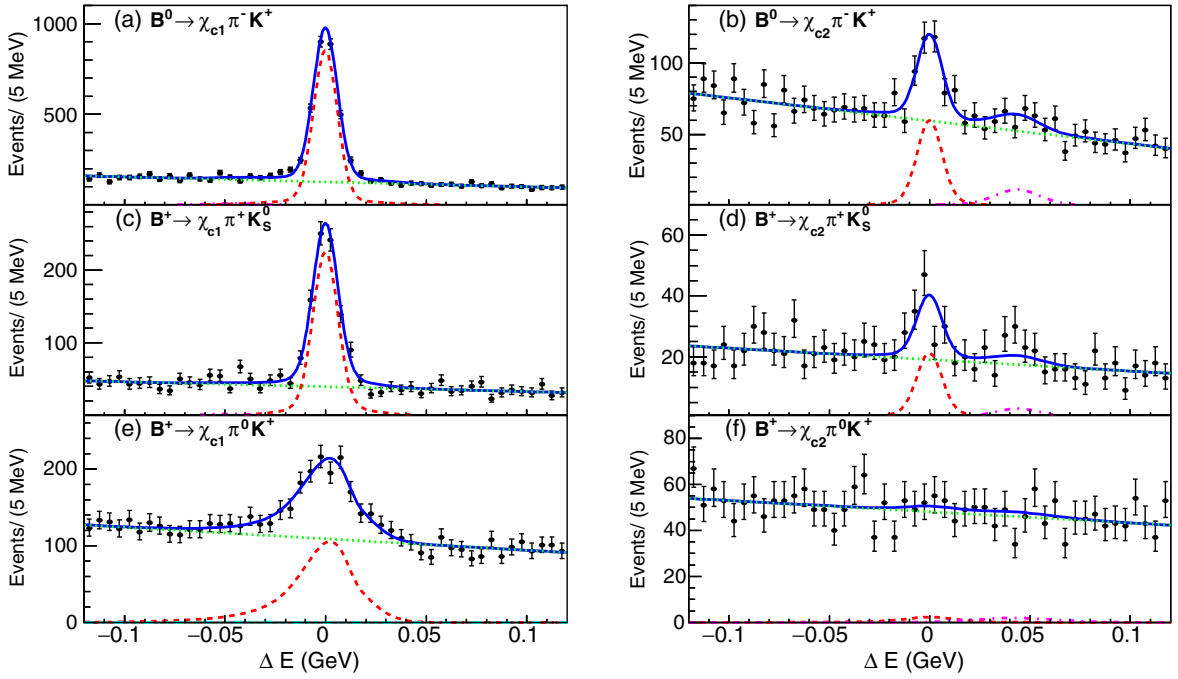

FIG. 3. ΔE distribution for the (a) $B^0 \to \chi_{c1}\pi^- K^+$, (b) $B^0 \to \chi_{c2}\pi^- K^+$, (c) $B^+ \to \chi_{c1}\pi^+ K^0_S$, (d) $B^+ \to \chi_{c2}\pi^+ K^0_S$, (e) $B^+ \to \chi_{c1}\pi^0 K^+$, and (f) $B^+ \to \chi_{c2}\pi^0 K^+$ decay modes. The curves show the signal (red dashed), the peaking background (magenta dash dotted) and the background component (green dotted for combinatorial) as well as the overall fit (blue solid).

decay modes having a significance of 67σ (8.7σ), 34σ (4.6σ) and 16σ (0.4σ), respectively. The significance is estimated using the value of $-2\ln(\mathcal{L}_0/\mathcal{L}_{\rm max})$, where $\mathcal{L}_{\rm max}$ ($\mathcal{L}_0$) denotes the likelihood value when the yield is allowed to vary (is set to zero). The systematic uncertainty, which is described below, is included in the significance calculation [31]. We make the first observation of the $B^0 \to \chi_{c2}\pi^- K^+$ decay mode along with the first evidence for a $B^+ \to \chi_{c2}\pi^+ K^0_S$ decay. We estimate the branching fractions according to the formula $\mathcal{B} = Y/(\epsilon \times \mathcal{B}_s \times N_{B\bar{B}})$; here Y is the yield, ϵ is the reconstruction efficiency, $\mathcal{B}_s$ is the secondary branching fraction taken from Ref. [8], and $N_{B\bar{B}}$ is the number of $B\bar{B}$ mesons in the data sample. Equal production of neutral and charged B meson pairs in the $\Upsilon(4S)$ decay is assumed. Table II summarizes the results.

The $K^*(892)$ is found to be a major contribution in the $B \to \chi_{c1}\pi K$ decay modes as seen from Figs. 4(a), 4(e) and 4(i); in $B \to \chi_{c2}\pi K$ decays, the $K^*(892)$ component is less prominent and a cluster of events around $M_{K^\pm\pi^\mp} = 1.4\ {\rm GeV}/c^2$ shows a relatively large contribution. Our study suggests that the $B \to \chi_{c2}K^*(892)$ mechanism does not dominate the $B \to \chi_{c2}\pi K$ decay, in marked contrast to the χ_{c1} case. Until now, the previous measurements of χ_{c2} [6,7] were limited to $B^0 \to \chi_{c2}K^*(892)^0$ only and so were not able to observe three-body B decays. From this study, one may posit that the production mechanism of the χ_{c2} from B mesons is different in three-body decays for the $B \to \chi_{c1}\pi K$ case. As shown in Figs. 4(b) and 4(f), the $M_{\chi_{c1}\pi^\pm}$ distributions are similar to those obtained by a previous Belle study [32] in which a Dalitz analysis suggested two charged Z states decaying into $\chi_{c1}\pi^+$. Also, the $M_{\chi_{c1}\pi^0}$ distribution in Fig. 4(j) shows a similar behavior as seen in the charged $M_{\chi_{c1}\pi^\pm}$ distribution. However, due to limited statistics, no noticeable feature in the $M_{\chi_{c2}\pi^+}$ spectrum is seen as shown in the corresponding Figs. 4(d) and 4(h).

In decay modes where we find no significant signal, we determine a 90% C.L. upper limit (U.L.) on its branching fraction with a frequentist method that uses ensembles of pseudoexperiments. For a given signal yield, 10000 sets of signal and background events are generated according to their PDFs and fits are performed. The U.L. is determined from the fraction of samples that gives a yield larger than that of data.

B. $B \to \chi_{cJ}\pi\pi K$

Each χ_{cJ} candidate is combined with a pair of oppositely charged pions (or a charged-neutral pair) and a kaon (either $K^\pm$ or K^0_S) to reconstruct the B decays of interest: $B^+ \to \chi_{cJ}\pi^+\pi^- K^+$, $B^0 \to \chi_{cJ}\pi^+\pi^- K^0_S$ and $B^0 \to \chi_{cJ}\pi^-\pi^0 K^+$ decay modes. Of the selected B candidates, identified by the ΔE and $M_{\rm bc}$ requirement, 35%, 35% and 50% have multiple candidates in the $B^+ \to \chi_{cJ}\pi^+\pi^- K^+$, $B^0 \to \chi_{cJ}\pi^+\pi^- K^0_S$ and $B^0 \to \chi_{cJ}\pi^-\pi^0 K^+$ decay modes, respectively. In case of multiple B candidates, the aforementioned BCS is used to select a single B candidate in the event.

The signal yield is extracted from a one-dimensional UML fit to the ΔE distribution as shown in Fig. 5. We get 1502 ± 70 (269 ± 34), 268 ± 30 (37.8 ± 14.2)

TABLE II. Summary of the results. Signal yield (Y) from the fit, significance ($\mathcal{S}$) with systematics included, corrected efficiency (ϵ) and measured $\mathcal{B}$. For $\mathcal{B}$, the first (second) error is statistical (systematic). Here, in the neutral B decay case, the $K^0_S \to \pi^+\pi^-$ branching fraction is included in the efficiency (ϵ) but the factor of 2 (for $K^0 \to K^0_S$ or K^0_L) is taken into account separately. $\mathcal{R}_\mathcal{B}$ is the ratio of $\mathcal{B}(B \to \chi_{c2}X)$ to $\mathcal{B}(B \to \chi_{c1}X)$, where X is the same set of particles accompanying the χ_{c1} (χ_{c2}) in the final states.

Decay	Yield (Y)	$\mathcal{S}(\sigma)$	$\epsilon(\%)$	$\mathcal{B}$ (10^{-4})	$\mathcal{R}_\mathcal{B}$
$B^0 \to \chi_{cJ}\pi^- K^+$					0.14 ± 0.02
χ_{c1}	2774 ± 66	66.7	17.9	$4.97 \pm 0.12 \pm 0.28$	
χ_{c2}	206 ± 25	8.7	16.2	$0.72 \pm 0.09 \pm 0.05$	
$B^+ \to \chi_{cJ}\pi^+ K^0$					0.20 ± 0.04
χ_{c1}	770 ± 35	33.7	8.6	$5.75 \pm 0.26 \pm 0.32$	
χ_{c2}	76.4 ± 14.7	4.6	7.5	$1.16 \pm 0.22 \pm 0.12$	
$B^+ \to \chi_{cJ}\pi^0 K^+$					< 0.21
χ_{c1}	803 ± 70	15.6	7.8	$3.29 \pm 0.29 \pm 0.19$	
χ_{c2}	17.5 ± 28.4	0.4	7.0	< 0.62	
$B^+ \to \chi_{cJ}\pi^+\pi^- K^+$					0.36 ± 0.05
χ_{c1}	1502 ± 70	19.2	12.8	$3.74 \pm 0.18 \pm 0.24$	
χ_{c2}	269 ± 34	8.4	11.4	$1.34 \pm 0.17 \pm 0.09$	
$B^0 \to \chi_{cJ}\pi^+\pi^- K^0$					< 0.61
χ_{c1}	268 ± 30	7.1	5.4	$3.16 \pm 0.35 \pm 0.32$	
χ_{c2}	37.8 ± 14.2	1.8	4.8	< 1.70	
$B^0 \to \chi_{cJ}\pi^-\pi^0 K^+$					< 0.25
χ_{c1}	545 ± 81	6.5	5.0	$3.52 \pm 0.52 \pm 0.24$	
χ_{c2}	-76.7 ± 42.0	...	4.3	< 0.74	

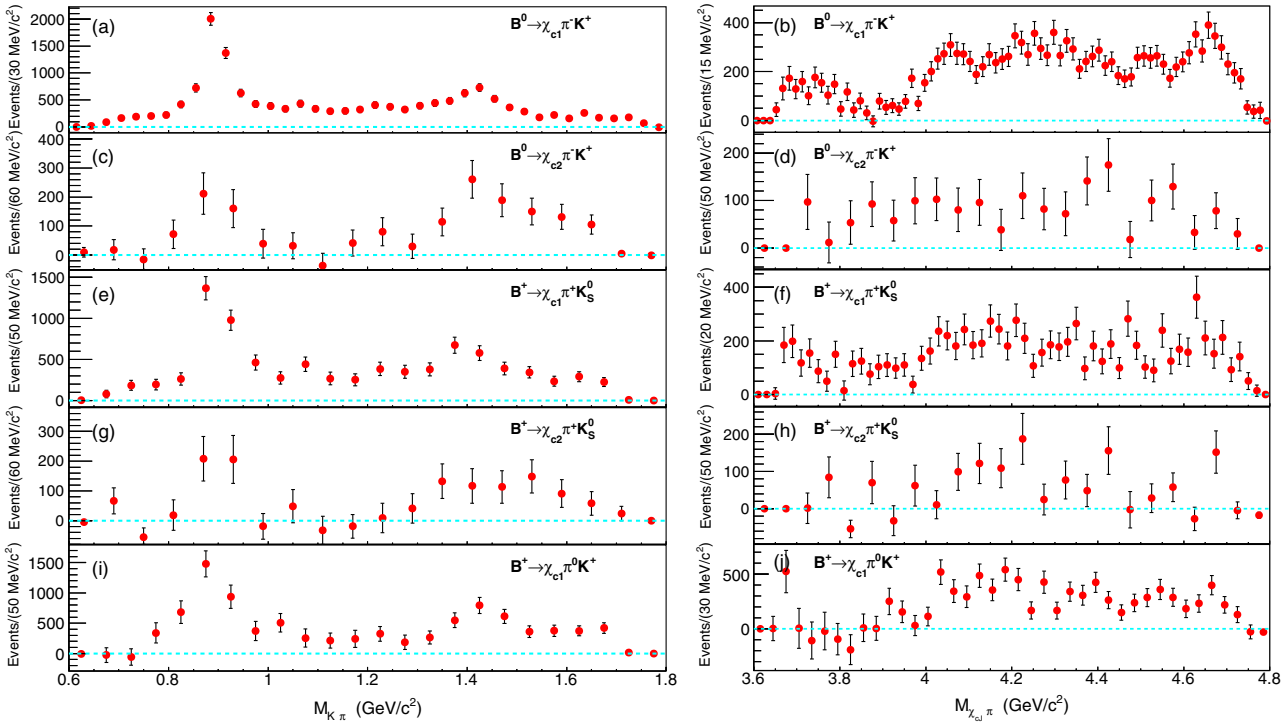

FIG. 4. Background subtracted efficiency corrected ${}_s\mathcal{P}lot$ $M_{K\pi}$ and $M_{\chi_{cJ}\pi}$ distributions for the (a–b) $B^0 \to \chi_{c1}\pi^- K^+$, (c–d) $B^0 \to \chi_{c2}\pi^- K^+$, (e–f) $B^+ \to \chi_{c1}\pi^+ K^0_S$, (g–h) $B^+ \to \chi_{c2}\pi^+ K^0_S$ and (i–j) $B^+ \to \chi_{c1}\pi^0 K^+$ decay modes.

and 545 ± 81 (-76.7 ± 42.0) signal events with a 19.2σ (8.4σ), 7.1σ (1.8σ) and 6.5σ (null) significance for the $B^+ \to \chi_{c1}\pi^+\pi^- K^+$ $(B^+ \to \chi_{c2}\pi^+\pi^- K^+)$, $B^0 \to \chi_{c1}\pi^+\pi^- K^0_S$ $(B^0 \to \chi_{c2}\pi^+\pi^- K^0_S)$ and $B^0 \to \chi_{c1}\pi^-\pi^0 K^+$ $(B^0 \to \chi_{c2}\pi^-\pi^0 K^+)$ decay modes, respectively. For the first time, we observe the $B^+ \to \chi_{c1}\pi^+\pi^- K^+$, $B^+ \to \chi_{c2}\pi^+\pi^- K^+$, $B^0 \to \chi_{c1}\pi^+\pi^- K^0_S$, and $B^0 \to \chi_{c1}\pi^-\pi^0 K^+$ decay modes. Table II summarizes the fit results.

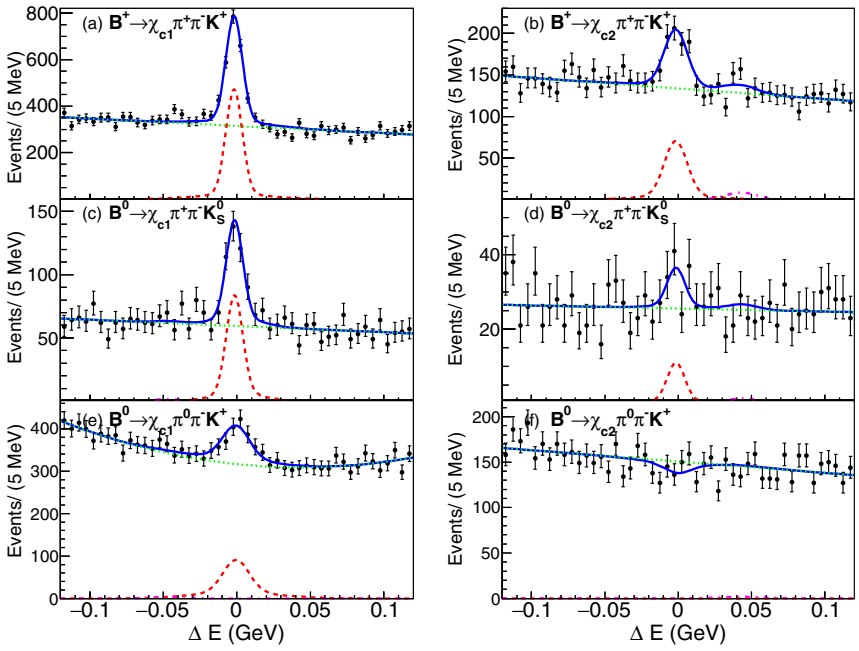

FIG. 5. ΔE distributions for the (a) $B^+ \to \chi_{c1}\pi^+\pi^- K^+$, (b) $B^+ \to \chi_{c2}\pi^+\pi^- K^+$, (c) $B^0 \to \chi_{c1}\pi^+\pi^- K^0_S$, (d) $B^0 \to \chi_{c2}\pi^+\pi^- K^0_S$, (e) $B^0 \to \chi_{c1}\pi^0\pi^- K^+$ and (f) $B^0 \to \chi_{c2}\pi^0\pi^- K^+$ decay modes. The curves show the signal (red dashed), peaking background (magenta dash dotted) and background component (green dotted for combinatorial) as well as the overall fit (blue solid).

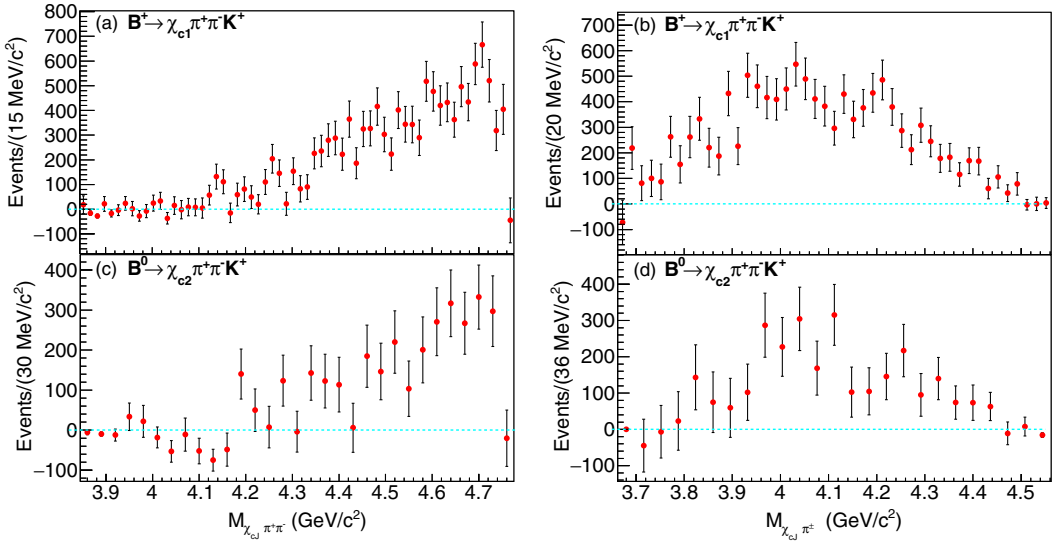

FIG. 6. Background subtracted efficiency corrected ${}_S\mathcal{P}lot$ (a) $M_{\chi_{c1}\pi^+\pi^-}$, (b) $M_{\chi_{c1}\pi^\pm}$, (c) $M_{\chi_{c2}\pi^+\pi^-}$ and (d) $M_{\chi_{c2}\pi^\pm}$ distributions for the $B^+ \to \chi_{cJ}\pi^+\pi^-K^+$ decay modes.

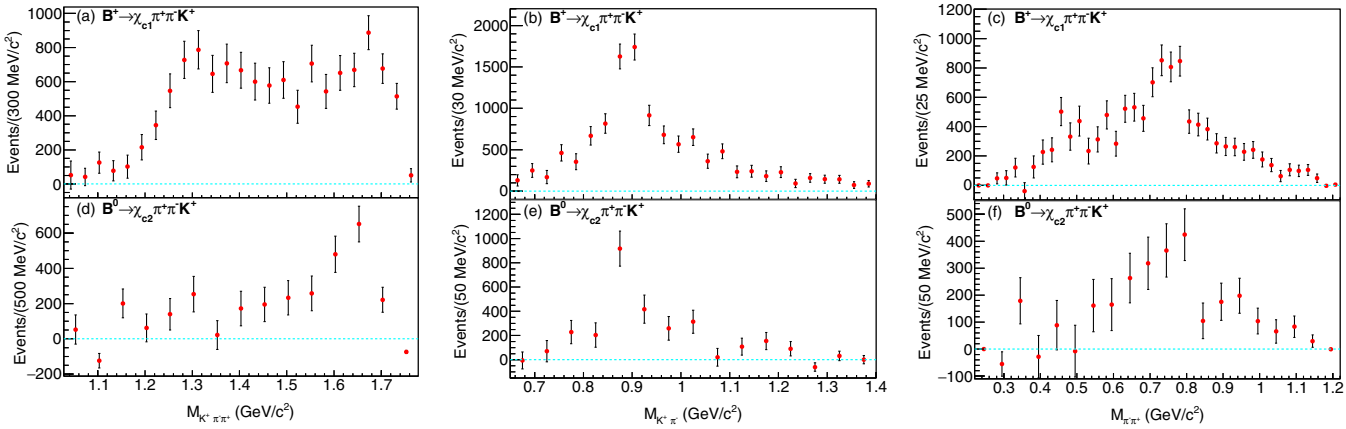

FIG. 7. Background subtracted efficiency corrected ${}_S\mathcal{P}lot$ (a and d) $M_{K^+\pi^+\pi^-}$, (b and e) $M_{K^+\pi^-}$ and (c and f) $M_{\pi^+\pi^-}$ distributions for $B^+ \to \chi_{c1}\pi^+\pi^-K^+$ decay (upper) and $B^+ \to \chi_{c2}\pi^+\pi^-K^+$ decay (lower), respectively.

In order to understand the dynamics of the production of χ_{cJ} in four-body B decays, we examine the background-subtracted ${}_S\mathcal{P}lot$ distribution of $M_{\chi_{cJ}\pi\pi}$, $M_{\chi_{cJ}\pi^\pm}$, $M_{K\pi\pi}$, $M_{K^+\pi^-}$, and $M_{\pi^+\pi^-}$, which are shown in Figs. 6–7 for the $B^+ \to \chi_{cJ}\pi^+\pi^-K^+$ decay mode. No narrow resonance can be seen in the $M_{\chi_{cJ}\pi^+\pi^-}$ and $M_{\chi_{cJ}\pi^\pm}$ distributions with the current statistics. There seems to be an enhancement of signal events around $4.1-4.2$ GeV/c^2 in $M_{\chi_{cJ}\pi\pi}$ that is due to cross feed; the same effect is seen in our $B \to J/\psi X$ MC sample that is used to study the background. Higher K^* resonances are seen in the $M_{K^+\pi^-\pi^+}$ and $M_{K^+\pi^-}$ distributions shown in Fig. 7 similar to the ones seen in the $B^+ \to J/\psi\pi^+\pi^-K^+$ decay mode [27]. There is a peaking structure near 1680 MeV/c^2 due to the $K^*(1680)^+$. Further, a $K^*(892)^0$ peak is found in $M_{K^+\pi^-}$. Here again, the contrast between $B^+ \to \chi_{c2}\pi^+\pi^-K^+$ decays and those to χ_{c1} is

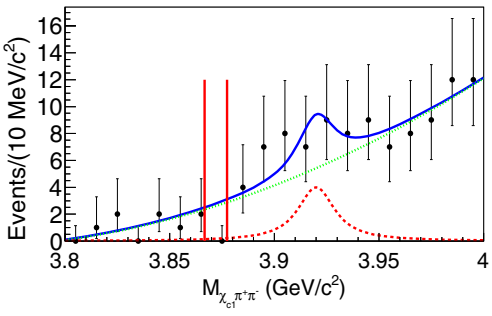

FIG. 8. The $\chi_{c1}\pi^+\pi^-$ invariant mass spectrum for $B^+ \to \chi_{c1}\pi^+\pi^-K^+$ candidates. Two vertical red lines show the $\pm 3\sigma$ window to search for $X(3872) \to \chi_{c1}\pi^+\pi^-$. The curves show the $\chi_{c1}(2P)$ signal (red dashed) and the background (green dotted) and the overall fit (blue solid).

apparent: the decays to χ_{c2} mostly include higher K^* resonances. Figures 7(e)–7(f) show the $M_{\pi^+\pi^-}$ distributions for the $B^+ \to \chi_{cJ}\pi^+\pi^-K^+$ decay mode, which suggest a contribution from ρ as an intermediate state.

C. Search for $X(3872)$ and $\chi_{c1}(2P)$

To search for the $X(3872) \to \chi_{c1}\pi^+\pi^-$, we investigate the signal in the $M_{\chi_{c1}\pi^+\pi^-}$ distribution within the signal-enhanced window of -20 MeV $< \Delta E < 20$ MeV for $B^+ \to \chi_{c1}\pi^+\pi^-K^+$ candidates. In the absence of any significant peak as shown in Fig. 8, we count the number of events within the $\pm 3\sigma$ window and find no events. Therefore, we use 2.6 events as the upper limit of the signal yield based on the Feldman and Cousins approach [33] including systematic uncertainty of the detection efficiency. Using 5.6% as the corrected efficiency for $B^+ \to X(3872)(\to \chi_{c1}\pi^+\pi^-)K^+$ estimated from signal MC, we obtain $\mathcal{B}(B^+ \to X(3872)K^+) \times \mathcal{B}(X(3872) \to \chi_{c1}\pi^+\pi^-) < 1.5 \times 10^{-6}$ (90% C.L.).

The $\chi_{c1}(2P)$ signal in the $M_{\chi_{c1}\pi\pi}$ spectrum is described by a PDF composed as the convolution of a Breit-Wigner function with a Gaussian. As a plausible assumption for the $\chi_{c1}(2P)$ state, its mass and width are fixed at 3920 MeV/c^2 and 20 MeV, assuming the PDG interpretation of $X(3915) = \chi_{c0}(2P)$ and the property of $\chi_{c2}(2P)$ [8]. The width of the Gaussian is fixed to 2 MeV, corresponding to the detector resolution in the mass estimation obtained from MC-simulated samples. The fit (shown in Fig. 8) results in a signal yield of 12.2 ± 9.1 events, which translates to 30.3 events at the 90% confidence level.

TABLE III. U.L. for $B^+ \to X(\to \chi_{c1}\pi^+\pi^-)K^+$; here X stands for $X(3872)$ and the assumed $\chi_{c1}(2P)$. The upper limit at 90% C.L. includes the systematics ($N^{U.L.}$), corrected efficiency (ϵ) and product of branching fractions $\mathcal{B}(B^+ \to XK^+) \times \mathcal{B}(X \to \chi_{c1}\pi^+\pi^-)$ ($\mathcal{B}^{U.L.}$).

Mode	$Y^{U.L.}$	ϵ (%)	$\mathcal{B}^{U.L.}$ ($\times 10^{-5}$)
$X(3872)$	< 2.6	5.6	< 0.15
$\chi_{c1}(2P)$	< 30.3	8.9	< 1.10

A product branching fraction upper limit is extracted, including statistical and systematic uncertainties and the 8.9% reconstruction efficiency: $\mathcal{B}(B^+ \to \chi_{c1}(2P)K^+) \times \mathcal{B}(\chi_{c1}(2P) \to \chi_{c1}(1P)\pi^+\pi^-) < 1.1 \times 10^{-5}$ (90% C.L.).

Table III summarizes our search for $X(3872)$ and $\chi_{c1}(2P)$ in the $B^+ \to (\chi_{c1}\pi^+\pi^-)K^+$ decay mode.

D. Systematics

Table IV summarizes the systematic for each mode. Corrections for small differences in the signal detection efficiency between MC and data have been applied for the lepton and kaon identification requirements, as was done in the inclusive study. In addition to the items commonly affecting the inclusive branching fraction measurements, we consider the following systematic uncertainty sources. In Belle, dedicated $D^{*+} \to D^0(K^-\pi^+)\pi^+$ samples are used to estimate the kaon (pion) identification efficiency correction. To estimate the correction and residual systematic uncertainty for K^0_S reconstruction,

TABLE IV. Summary of systematic uncertainties on the $B \to \chi_{cJ}X$ branching fraction: uncertainty on lepton identification (ℓ), kaon identification (K), pion identification (π), tracking, gamma identification (γ id), K^0_S reconstruction, π^0 reconstruction, π^0 veto, uncertainty in the secondary branching fractions, PDFs used to extract signal yield and uncertainty on the $N_{B\bar{B}}$.

	Uncertainty (%)												
Mode	ℓ	K	π	Tracking	γ id	Secondary $\mathcal{B}$	K^0_S	π^0	π^0 veto	ϵ	PDF	$N_{B\bar{B}}$	Total
$B^0 \to \chi_{cJ}\pi^-K^+$													
χ_{c1}	2.1	1.0	1.0	1.4	2.0	3.6	⋯	⋯	1.2	1.0	1.4	1.4	5.6
χ_{c2}	2.1	1.0	1.0	1.4	2.0	3.7	⋯	⋯	1.2	2.4	3.2	1.4	6.7
$B^+ \to \chi_{cJ}\pi^+K^0$													
χ_{c1}	2.1	⋯	1.0	1.8	2.0	3.6	0.7	⋯	1.2	1.0	0.7	1.4	5.5
χ_{c2}	2.1	⋯	1.1	1.8	2.0	3.7	0.7	⋯	1.2	2.2	9.1	1.4	10.8
$B^+ \to \chi_{cJ}\pi^0K^+$													
χ_{c1}	2.1	1.0	⋯	1.1	2.0	3.6	⋯	2.2	1.2	1.0	1.7	1.4	5.9
χ_{c2}	2.1	1.0	⋯	1.1	2.0	3.7	⋯	2.2	1.2	2.4	191	1.4	191.1
$B^+ \to \chi_{cJ}\pi^+\pi^-K^+$													
χ_{c1}	2.1	1.1	2.3	1.8	2.0	3.6	⋯	⋯	1.2	1.0	2.6	1.4	6.5
χ_{c2}	2.1	1.2	2.3	1.8	2.0	3.7	⋯	⋯	1.2	2.2	2.0	1.4	6.6
$B^0 \to \chi_{cJ}\pi^+\pi^-K^0$													
χ_{c1}	2.1	⋯	2.3	2.1	2.0	3.6	0.7	⋯	1.2	1.0	8.1	1.4	10.1
χ_{c2}	2.1	⋯	2.3	2.1	2.0	3.7	0.7	⋯	1.2	2.3	31.5	1.4	32.1
$B^0 \to \chi_{cJ}\pi^-\pi^0K^+$													
χ_{c1}	2.1	1.1	1.1	1.4	2.0	3.6	⋯	2.2	1.2	1.1	3.6	1.4	6.9
χ_{c2}	2.1	1.2	1.1	1.4	2.0	3.7	⋯	2.2	1.2	2.9	**	1.4	7.5

$D^{*+} \to D^0(\to K^0_S\pi^+\pi^-)\pi^+$ samples are used. For π^0, the efficiency correction and systematic uncertainty are estimated from a sample of $\tau^- \to \pi^+\pi^0\nu_\tau$ decays. The errors on the PDF shapes are obtained by varying all fixed parameters by $\pm 1\sigma$ and taking the change in the yield as the systematic uncertainty.

E. Discussion on exclusive decays

Table II summarizes the studied exclusive decays of B to $\chi_{cJ}X$ decays. For the first time, we observe the $B^0 \to \chi_{c2}\pi^-K^+$, $B^+ \to \chi_{c2}\pi^+K^0_S$, $B^+ \to \chi_{c2}\pi^+\pi^-K^+$, $B^+ \to \chi_{c1}\pi^+\pi^-K^+$, $B^0 \to \chi_{c1}\pi^+\pi^-K^0$ and $B^0 \to \chi_{c1}\pi^-\pi^0K^+$ decay modes. We find that in three-body decays the χ_{c2} is more likely to be produced in association with higher K^* resonances; in contrast, decays to χ_{c1} are accompanied predominantly by the $K^*(892)$. The same phenomenon is observed in the four-body production of χ_{c2} and χ_{c1} from B decays. No strong hint for any narrow resonance (less than 5 MeV width) is seen in the $M_{\chi_{cJ}\pi}$ and $M_{\chi_{cJ}\pi\pi}$ distributions. If one adds the measured branching fraction in this paper (excluding the obtained U.L.), we obtain $\mathcal{B}(B \to \chi_{c1}n\pi K)$ with $n \in \{1,2\}$ to be $(1.75 \pm 0.08) \times 10^{-3}$, which corresponds to a $(58 \pm 5)\%$ fraction of the measured $\mathcal{B}(B \to \chi_{c1}X)$. Using $\mathcal{B}(B^+ \to \chi_{c1}K^+)$ [8], this accounts for $(74 \pm 6)\%$ of B mesons decaying into $\chi_{c1}X$. Similarly, $\mathcal{B}(B \to \chi_{c2}n\pi K)$ with $n \in \{1,2\}$ is $(0.23 \pm 0.02) \times 10^{-3}$, corresponding to $(32 \pm 5)\%$ of the inclusive $\mathcal{B}(B \to \chi_{c2}X)$. For the treatment of the uncertainty, no correlation is assumed and the uncertainty is the sum of the systematic and statistical uncertainties in quadrature.

VI. SUMMARY

We measured the feed down-contaminated $\mathcal{B}(B \to \chi_{c1}X)$ and $\mathcal{B}(B \to \chi_{c2}X)$ of $(3.33 \pm 0.05 \pm 0.24) \times 10^{-3}$ and $(0.98 \pm 0.06 \pm 0.10) \times 10^{-3}$, respectively, where the first (second) error is statistical (systematic). After subtracting the ψ' feed down contributions, we find the pure inclusive branching fractions $\mathcal{B}(B \to \chi_{c1}X)$ and $\mathcal{B}(B \to \chi_{c2}X)$ of $(3.03 \pm 0.05 \pm 0.24) \times 10^{-3}$ and $(0.70 \pm 0.06 \pm 0.10) \times 10^{-3}$, respectively. Here, the systematic uncertainty dominates. For inclusive production of χ_{cJ}, we measure the ratio $\mathcal{B}(B \to \chi_{c2}X)/\mathcal{B}(B \to \chi_{c1}X)$ of $(23.1 \pm 2.0 \pm 2.1)\%$. We observe the $B^0 \to \chi_{c2}\pi^-K^+$ decay mode for the first time, with 206 ± 25 signal events and a significance of 8.7σ, along with evidence for the $B^+ \to \chi_{c2}\pi^+K^0_S$ decay mode, with 76 ± 15 signal events and a significance of 4.6σ. In four-body decays, we observe the $B^+ \to \chi_{c1}\pi^+\pi^-K^+$, $B^+ \to \chi_{c1}\pi^+\pi^-K^+$, $B^0 \to \chi_{c1}\pi^+\pi^-K^0_S$, and $B^0 \to \chi_{c1}\pi^0\pi^-K^+$ decay modes for the first time and report on measurements of their branching fractions. We find that χ_{c2} production, in contrast with χ_{c1}, increases with a higher number of multibody B decays: $\mathcal{R}_\mathcal{B}$ for $B^+ \to \chi_{cJ}\pi^+\pi^-K^+$ decay (0.36 ± 0.05) is almost twice that measured in the $B^0 \to \chi_{cJ}\pi^-K^+$ decay mode (0.20 ± 0.04). We observe that the χ_{c2} is more often accompanied by higher K^* resonances, in contrast to the χ_{c1} that is dominantly produced with the lower K^* resonance. All previous studies [6,7] were limited to $K^*(892)^0$, while our study suggests that χ_{c2} is preferentially produced with higher K^* resonances. Clearly, to study χ_{c2} production in B decays, it is important to avoid considering solely the lower K^* resonances. Suppression in two-body B decays is found to be due to the factorization hypothesis [9]. In our search for $X(3872) \to \chi_{c1}\pi^+\pi^-$ and $\chi_{c1}(2P)$, we determine an U.L. on the product of branching fractions $\mathcal{B}(B^+ \to X(3872)K^+) \times (X(3872) \to \chi_{c1}\pi^+\pi^-)$ $[\mathcal{B}(B^+ \to \chi_{c1}(2P)K^+) \times (\chi_{c1}(2P) \to \chi_{c1}\pi^+\pi^-)] < 1.5 \times 10^{-6}$ $[1.1 \times 10^{-5}]$ at the 90% C.L. The negative result for our searches is compatible with the interpretation of $X(3872)$ as an admixture state of a $D^0\bar{D}^{*0}$ molecule and a $\chi_{c1}(2P)$ charmonium state.

ACKNOWLEDGMENTS

We thank the KEKB group for the excellent operation of the accelerator; the KEK cryogenics group for the efficient operation of the solenoid; and the KEK computer group, the National Institute of Informatics, and the PNNL/EMSL computing group for valuable computing and SINET4 network support. We acknowledge support from the Ministry of Education, Culture, Sports, Science, and Technology (MEXT) of Japan, the Japan Society for the Promotion of Science (JSPS), and the Tau-Lepton Physics Research Center of Nagoya University; the Australian Research Council; Austrian Science Fund under Grants No. P 22742-N16 and No. P 26794-N20; the National Natural Science Foundation of China under Contracts No. 10575109, No. 10775142, No. 10875115, No. 11175187, and No. 11475187; the Chinese Academy of Science Center for Excellence in Particle Physics; the Ministry of Education, Youth and Sports of the Czech Republic under Contract No. LG14034; the Carl Zeiss Foundation, the Deutsche Forschungsgemeinschaft and the VolkswagenStiftung; the Department of Science and Technology of India; the Istituto Nazionale di Fisica Nucleare of Italy; the WCU program of the Ministry of Education, National Research Foundation (NRF) of Korea Grants No. 2011-0029457, No. 2012-0008143, No. 2012R1A1A2008330, No. 2013R1A1A3007772, No. 2014R1A2A2A01005286, No. 2014R1A2A2A01002734, No. 2015R1A2A2A01003280, and No. 2015H1A2A1033649; the Basic Research Lab program under NRF Grant No. KRF-2011-0020333, Center for Korean J-PARC Users, Grant No. NRF-2013K1A3A7A06056592; the Brain Korea 21-Plus program and Radiation Science Research Institute; the Polish Ministry of Science and Higher Education and the National Science Center; the

Ministry of Education and Science of the Russian Federation and the Russian Foundation for Basic Research; the Slovenian Research Agency; the Basque Foundation for Science (IKERBASQUE) and the Euskal Herriko Unibertsitatea (UPV/EHU) under program Grant No. UFI 11/55 (Spain); the Swiss National Science Foundation; the National Science Council and the Ministry of Education of Taiwan; and the U.S. Department of Energy and the National Science Foundation. This work is supported by a Grant-in-Aid from MEXT for Science Research in a Priority Area ("New Development of Flavor Physics"), for Scientific Research on Innovative Areas ("Elucidation of New Hadrons with a Variety of Flavors"), and from JSPS for Creative Scientific Research ("Evolution of Tau-lepton Physics").

[1] K. Abe *et al.* (Belle Collaboration), Phys. Rev. Lett. **89**, 011803 (2002).
[2] Hereinafter, χ_{cJ} refers to either χ_{c1} or χ_{c2}, depending on which is reconstructed.
[3] B. Aubert *et al.* (*BABAR* Collaboration), Phys. Rev. D **67**, 032002 (2003).
[4] V. Bhardwaj *et al.* (Belle Collaboration), Phys. Rev. Lett. **107**, 091803 (2011).
[5] N. Soni *et al.* (Belle Collaboration), Phys. Lett. B **634**, 155 (2006).
[6] B. Aubert *et al.* (*BABAR* Collaboration), Phys. Rev. Lett. **102**, 132001 (2009).
[7] R. Aaij *et al.* (LHCb Collaboration), Nucl. Phys. **B874**, 663 (2013).
[8] K. A. Olive *et al.* (Particle Data Group), Chin. Phys. C **38**, 090001 (2014).
[9] J. H. Kühn, S. Nussinov, and R. Rückl, Z. Phys. C, **5**, 117 (1980); G. T. Bodwin, E. Braaten, T. C. Yuan, and G. P. Lepage, Phys. Rev. D **46**, R3703 (1992).
[10] A. Abulencia *et al.* (CDF Collaboration), Phys. Rev. Lett. **98**, 132002 (2007).
[11] S.-K. Choi *et al.* (Belle Collaboration), Phys. Rev. D **84**, 052004 (2011).
[12] R. Aaij *et al.* (LHCb Collaboration), Phys. Rev. Lett. **110**, 222001 (2013).
[13] E. Braaten and M. Kusunoki, Phys. Rev. D **69**, 074005 (2004); Y.-B. Dong, A. Faessler, T. Gutsche, and V. E. Lyubovitskij, Phys. Rev. D **77**, 094013 (2008).
[14] A. Abashian *et al.* (Belle Collaboration), Nucl. Instrum. Methods Phys. Res., Sect. A **479**, 117 (2002); also see detector section in J. Brodzicka *et al.*, Prog. Theor. Exp. Phys. **2012**, 04D001 (2012).
[15] S. Kurokawa and E. Kikutani, Nucl. Instrum. Methods Phys. Res., Sect. A **499**, 1 (2003), and other papers included in this volume; T. Abe *et al.*, Prog. Theor. Exp. Phys. **2013**, 03A001 (2013) and following articles up to 03A011.
[16] Z. Natkaniec *et al.* (Belle SVD2 Group), Nucl. Instrum. Methods Phys. Res., Sect. A **560**, 1 (2006).
[17] K. Abe *et al.* (Belle Collaboration), Phys. Rev. D **67**, 032003 (2003).
[18] G. C. Fox and S. Wolfram, Phys. Rev. Lett. **41**, 1581 (1978).
[19] D. J. Lange, Nucl. Instrum. Methods Phys. Res., Sect. A **462**, 152 (2001).
[20] E. Barberio and Z. Wąs, Comput. Phys. Commun. **79**, 291 (1994).
[21] R. Brun *et al.*, GEANT3.21, CERN Report No. DD/EE/84-1, 1984.
[22] P. Koppenburg *et al.* (Belle Collaboration), Phys. Rev. Lett. **93**, 061803 (2004).
[23] T. Skwarnicki, Ph.D. thesis, Institute for Nuclear Physics, Krakow, 1986; DESY Report No. DESY F31-86-02, 1986.
[24] The double-sided Crystal Ball function is defined as

$$\begin{aligned} f(x) &= N_0(n_l/|\alpha_l|)^{n_l}\exp(-|\alpha_l|^2/2) \\ &\quad\times[n_l/|\alpha_l| - |\alpha_l| - (x-\mu)/\sigma]^{-n_l}, \\ &\quad \text{if } (x-\mu)/\sigma \le -\alpha_l \\ &= N_0(n_r/|\alpha_r|)^{n_r}\exp(-|\alpha_r|^2/2) \\ &\quad\times[n_r/|\alpha_r| - |\alpha_r| + (x-\mu)/\sigma]^{-n_r}, \\ &\quad \text{if } (x-\mu)/\sigma \ge \alpha_r \\ &= N_0\exp[-(x-\mu)^2/(2\sigma^2)], \quad \text{otherwise.} \end{aligned}$$

Here N_0 is the normalization, σ is the standard deviation, μ is the mean, n_l (n_r), and α_l (α_r) are shape parameters for the left (right) tail.
[25] Charge-conjugate and neutral modes are included throughout the paper unless stated otherwise.
[26] H. Kakuno, Ph.D. thesis, Tokyo Institute of Technology, 2003, http://belle.kek.jp/belle/theses/doctor/kakuno03/kakuno_thesis.ps.gz.
[27] H. Guler *et al.* (Belle Collaboration), Phys. Rev. D **83**, 032005 (2011).
[28] K.-F. Chen *et al.* (Belle Collaboration), Phys. Rev. D **72**, 012004 (2005).
[29] M. Pivk and F. R. Le Diberder, Nucl. Instrum. Methods Phys. Res., Sect. A **555**, 356 (2005).
[30] The logarithmic Gaussian is parametrized as $f(x) = N_0/c \times \exp -\{\ln[(\epsilon - x)/(\epsilon - x_p)]\}^2/(2\sigma_0^2)$ where $\epsilon = \sigma/a + x_p$, $c = \sqrt{2\pi}\sigma_0(\epsilon - x)$ and $\sigma_0 = (\ln(a\sqrt{2\ln 2} + \sqrt{1+2a^2\ln 2})/\sqrt{2\ln 2}$. Here, N_0 is the normalization, σ is the standard deviation, x_p is the mean and a is the asymmetry.
[31] R. D. Cousins and V. L. Highland, Nucl. Instrum. Methods Phys. Res., Sect. A **320**, 331 (1992).
[32] R. Mizuk *et al.* (Belle Collaboration), Phys. Rev. D **78**, 072004 (2008).
[33] G. J. Feldman and R. D. Cousins, Phys. Rev. D **57**, 3873 (1998).